Electronic Supplementary Material (ESI) for Physical Chemistry Chemical Physics.
This journal is © the Owner Societies 2019

Electronic Supplementary Information

Water Dissociation and Hydrogen Evolution on Fe-based Bulk Metallic Glasses Surface

Ping-Ping Sun,[1] Devesh R. Kripalani,[1] Kun Zhou[1,2]*

[1]Singapore Centre for 3D Printing, School of Mechanical and Aerospace Engineering, Nanyang Technological University, 50 Nanyang Avenue, Singapore 639798, Singapore

[2] Environmental Process Modelling Centre, Nanyang Environment and Water Research Institute, Nanyang Technological University, 1 CleanTech Loop, Singapore 637141, Singapore

***Corresponding author.**

School of Mechanical and Aerospace Engineering

Nanyang Technological University

Singapore 639798, Singapore

Email address: kzhou@ntu.edu.sg

Telephone: +65 6790 5549 | Fax: +65 6792 4062

Note S1. Geometry stability and AIMD calculations of Fe-based BMG

To simulate the amorphous structure of the Fe-based BMG $Fe_{48}Cr_{15}Mo_{14}C_{15}B_6Y_2$, an initial structure is created using a periodic cell containing 45 Fe atoms, of which 22 Fe atoms are substituted by 6 C, 3 B, 6 Mo, 6 Cr and 1 Y atoms, consistent with the reported composition. As shown by Arora et al. through their energy dispersive spectroscopy (EDS) results, for Fe-rich BMG $Fe_{48}Cr_{15}Mo_{14}C_{15}B_6Y_2$, Fe, Mo and Cr elements have a higher probability than C, B and Y to be present across the coating interface.[1] Here, four different models, with the top-most layer consisting of only Fe atoms, binary composite elements Fe-Mo and Fe-Cr, and ternary composite elements Fe-Mo-Cr, are built to find the most energetically stable configuration of the Fe-rich phase.

Subsequently, AIMD calculations in the NVT ensemble are performed to emulate the processing steps of the experimental approach to approximately get the actual amorphous structures. In the MD calculations, the temperature is first increased from 0 K to 2000 K in 100 K increments, which is well-within the reported temperature range of 1773-2473 K for maintaining the structure in a semi-solid state.[2] Then, a single MD calculation is carried out to allow the structure to fully equilibrate at this temperature for about 10 ps long with the time step set at 1 fs. Next, the structure is quenched to room temperature (300 K) in 100 K decrements at a rate of 10 K/ps to achieve the high speed cooling effect necessary for obtaining amorphous structures.[3] Finally, another MD calculation is performed over 10 ps for the structure to reach thermal equilibrium at room temperature. All calculations are conducted at the Γ point with a single k point. The AIMD simulation evolution pathway is shown in Fig. S1a. Subsequently, the atomic coordinates and length of the lattice cell of all constructed models are fully relaxed with an atomic tolerance of 0.01 eV/Å. The tolerance for changes to the total energy is less than 1.0×10^{-5} eV.

On comparing the four different models, it is found that for the phases with the top-most layer composed of both binary and ternary composite elements, both Mo and Cr atoms tend to migrate to the inner layers, leaving the top-most layer with an iron-rich atomic distribution. Furthermore, a comparison on the optimization energy indicates that the stability of the four models is in the order of the top-most layer containing: only Fe atoms > binary Fe-Cr > ternary Fe-Mo-Cr > binary Fe-Mo. Previous investigation has also shown that the existence of Cr and Mo species will provide corrosion resistance.[4] However, when such corrosion resistance-enhancing elements are in the top-most layer, they will be oxidized by oxygen and lift off from the surface. Instead, it is when they are within the subsurface or inner layers, that they will exhibit the protective behavior observed experimentally.[5] Hence, it seems that the model with the top-most layer consisting of only Fe atoms will be more meaningful for this study (rather than the binary Fr-Cr model) given its superior oxidation stability under atmospheric conditions.

In experimental analysis, X-ray and neutron diffraction via reduced radial distribution functions (RDF) are straightforward methods to study the atomic structures of BMGs. To establish good agreement with experimental results, a clear relationship between the structural model and physical properties is necessary for validating the configurations obtained from MD simulations. Here, the XRD and RDF profiles of the most energetically stable model of the Fe-based BMG are simulated and shown in Fig. S1b–c. It is shown that several obvious peaks appear in the 2θ range between 20–100° of the XRD profile (Fig. S1b), which is consistent with previous experimental XRD results of the Fe-based BMG.[6, 7] This indicates that our model of the Fe-based BMG in the amorphous state can accurately represent the atomic arrangement of $Fe_{48}Cr_{15}Mo_{14}C_{15}B_6Y_2$ BMG used in relevant experiments. For the RDF result, the first peak at around 2 Å is mainly from the contribution between the transition metals (Fe/Cr/Mo) and C/B elements, while the second peak is mainly from the contribution of transition metals. The wave crests in the range of 4–7 Å are the results of hybridization of all atoms. Since no experimental RDF results are available for $Fe_{48}Cr_{15}Mo_{14}C_{15}B_6Y_2$ BMG, our simulated result is compared with the experimental RDF reported for an analogous constituent BMG $Fe_{49}Cr_{15}Mo_{14}C_{15}B_6Er_1$,[8] for which similar peak shapes and positions can be found. According to the XRD and RDF results, our model of the Fe-based BMG appears to correspond well and realistically with $Fe_{48}Cr_{15}Mo_{14}C_{15}B_6Y_2$ BMG in experiment.

Thus, the most energetically stable model with the top-most layer containing only Fe atoms will be taken as the research subject for the following calculations. Hereon, an investigation on its structural stability under the effect of thermal fluctuation is of great significance. The structural stability at each temperature can be evaluated by the root-mean-square deviation (RMSD) and root-mean-square fluctuation (RMSF) obtained from MD calculations.[9] The RMSD is defined as $(\sum(r_\mathrm{i} - r_0)^2/\mathrm{N})^{1/2}$, where r_i is the element position at time i, and r_0 is the reference value. The RMSF can be expressed as $(\sum(r_\mathrm{i} - \langle r\rangle)^2/\mathrm{N})^{1/2}$, where $\langle r\rangle$ is the average position.

The optimization energy (Fig. S1d), RMSD and RMSF (Fig. S1e-f) are calculated at both 2000 K and 300 K. At 2000 K, the energy drops to a convergent value within the first 2 ps along the simulation pathway, which means that the atoms are relaxing around their coordinates and the structure tends to achieve its equilibrium state. Besides, the trajectories of both RMSD and RMSF at 2000 K oscillate around an equilibrium value of 1.3 and 4Å, respectively. The regular oscillations indicate that the Fe-based BMG can reach a stable geometry at this temperature with sufficient timesteps. After quenching to 300 K, the energy waveform retains the same shape during the whole simulation duration, and both the RMSD and RMSF trajectories show much lower fluctuation intensity than those at 2000 K, suggesting that it can exhibit good stability at room temperature.

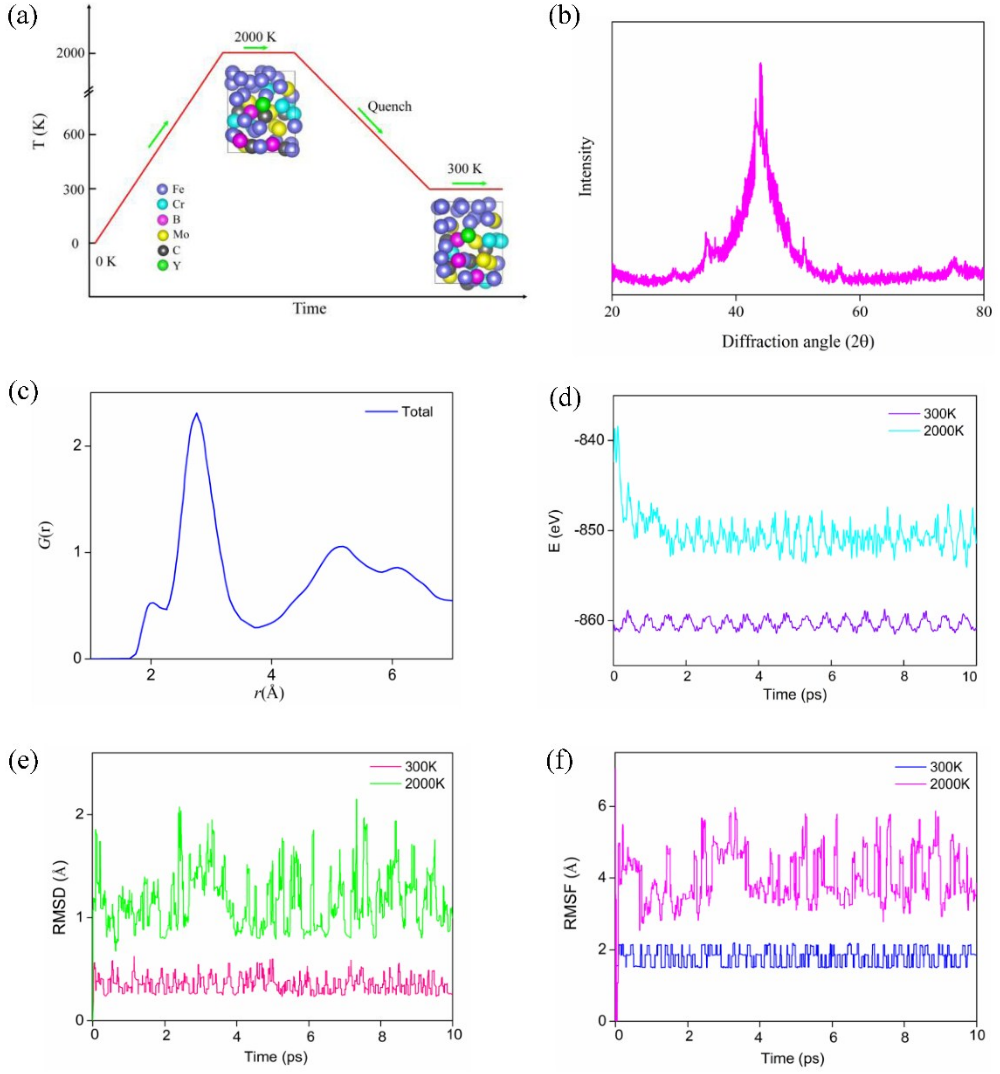

Fig. S1 (a) MD simulation evolution path of the Fe-based BMG. The representative structure of the Fe-based BMG is obtained by first increasing the temperature from 0 K to 2000 K in 100 K increments, after which, a single MD calculation is carried out to allow the structure to fully equilibrate at this temperature for a simulation time of 10 ps with the time step set at 1 fs. Then, it is quenched to room temperature (300 K) in 100 K decrements, followed by another single MD calculation to allow the structure to fully equilibrate at 300 K for a simulation time of 10 ps. The embedded figures are the relaxed structure under each specified temperature. (b) The simulated XRD pattern and (c) radial distribution function (RDF) of the total model for the Fe-based BMG. (d) Trajectories of the optimization energy at 300 K and 2000 K. Trajectories of the (e) RMSD and (f) RMSF with respect to the structure at 2000 K and 300 K.

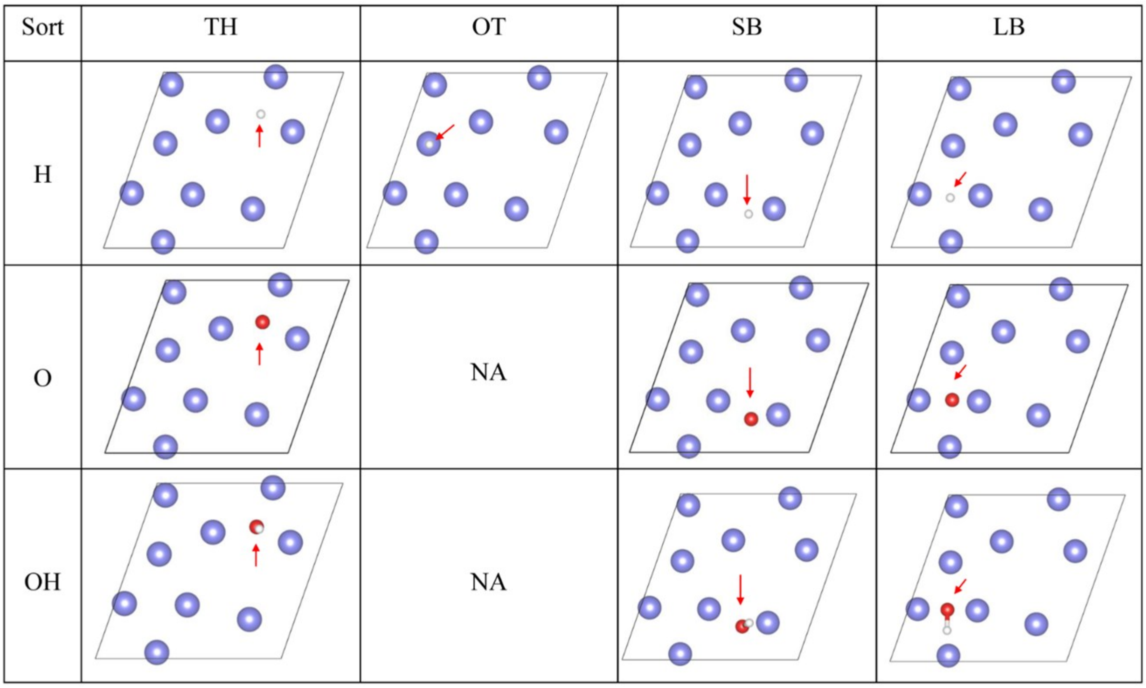

Fig. S2 The most stable configuration of H, O and OH groups on the BMG surface at the TH, OT, SB and LB adsorption sites. The red arrows point to the site with the H/O/OH group. To clearly show the sites of the adsorbates on the surface, only the first layer of Fe atoms and the adsorbates are presented.

Sort	H_2O				OH+H
Fe	TH	OT	SB	LB	LB+TH
	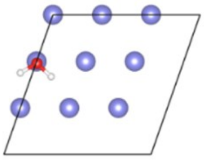	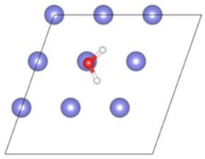	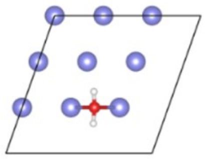	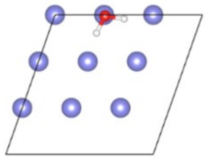	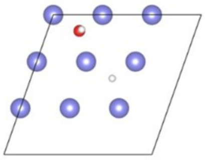
	*E*ads = −0.693 eV	*E*ads = −0.692 eV	*E*ads = −0.444 eV	*E*ads = − 0.686 eV	*E*ads = −1.763 eV
BMG	TH	OT	SB	LB	SB+SB
	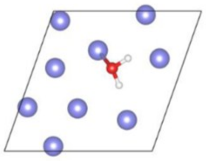	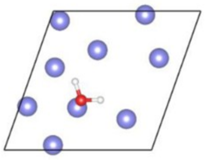	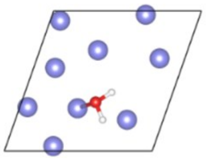	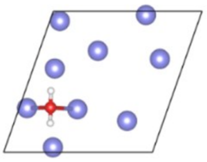	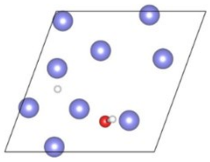
	*E*ads = −0.739 eV	*E*ads = −0.752 eV	*E*ads = −0.743 eV	*E*ads = −0.699 eV	*E*ads = −2.181 eV

Fig. S3 The configurations of H_2O at different sites and the final configuration of OH+H on the Fe and BMG surfaces. Before optimization, H_2O is initially placed at the TH, OT, SB and LB sites on both Fe and BMG surfaces. After optimization, on the Fe surface, H_2O migrates from the TH and LB sites to the OT site, while on the BMG surface, H_2O moves away from the initial TH and SB sites. On comparing the adsorption energies across configurations, H_2O prefers to adsorb at the OT site on both Fe and BMG surfaces.

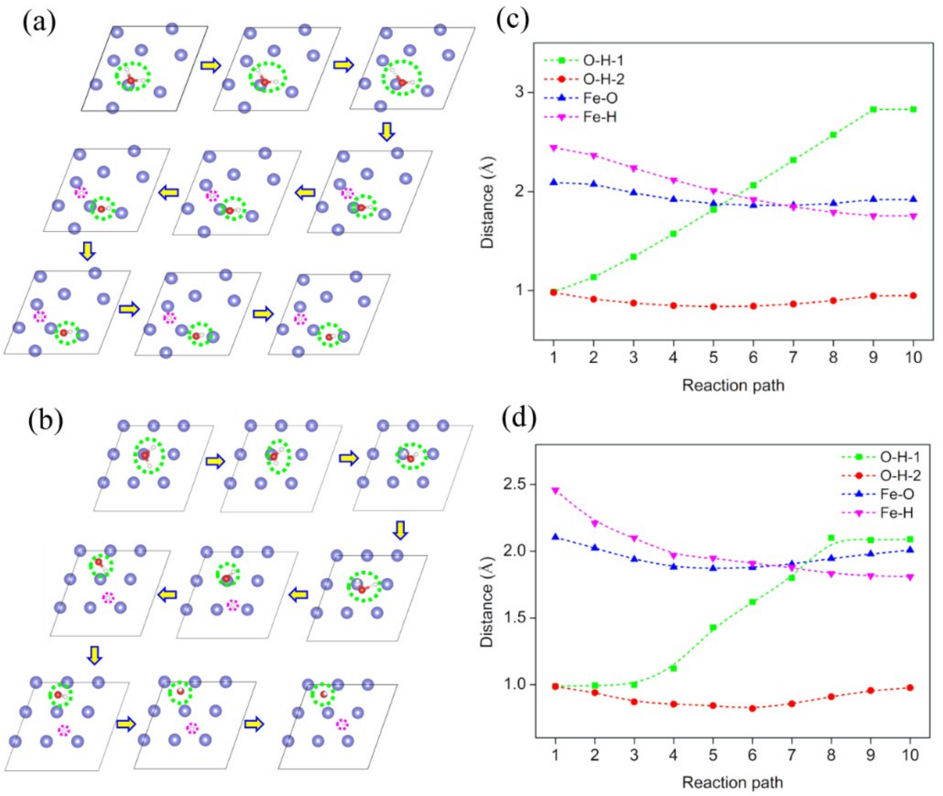

Fig. S4 Intermediate configurations in the dissociation reaction from H_2O to H+OH on the (a) BMG surface and (b) Fe surface, where only the first layer of Fe atoms and the adsorbates are shown. The pink circles represent H atoms and green circles indicate the OH/H_2O groups. Variation in O-H-1, O-H-2, Fe-O and Fe-H bond distances during the reaction path on the (c) BMG surface and (d) Fe surface.

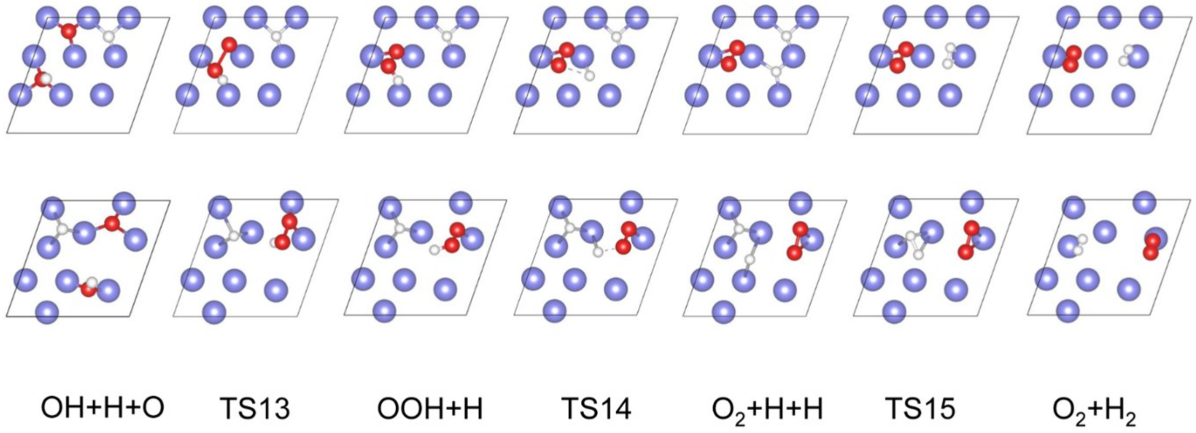

Fig. S5 Structural geometry along the dissociation path (b) from OH+H+O to O_2+H_2 through TS13-15 on the Fe surface (upper layer) and BMG surface (lower layer).

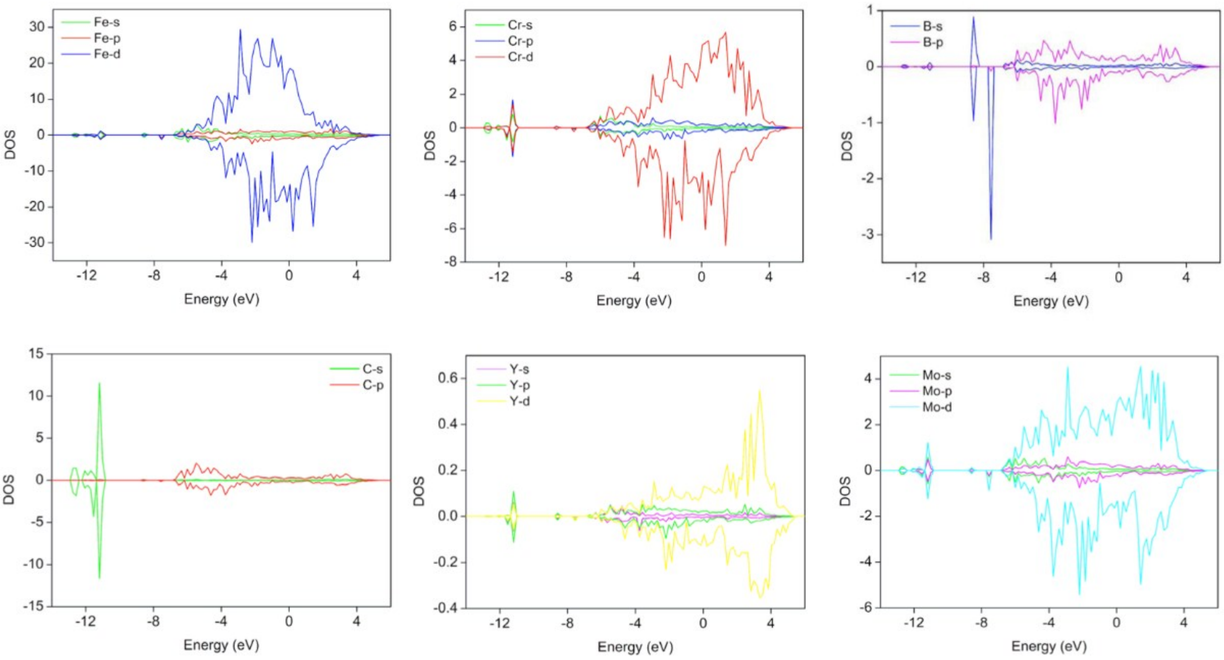

Fig. S6 PDOS structures of each atom in the BMG phase.

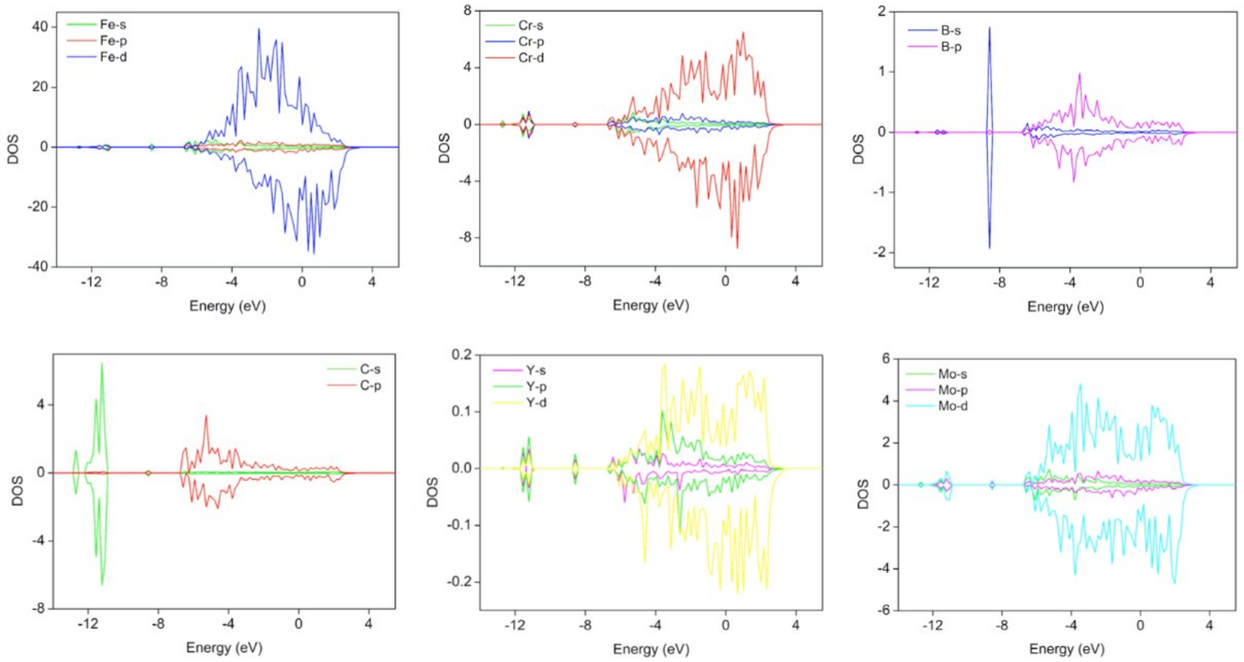

Fig. S7 PDOS structures of each atom in the H_2O-BMG phase.

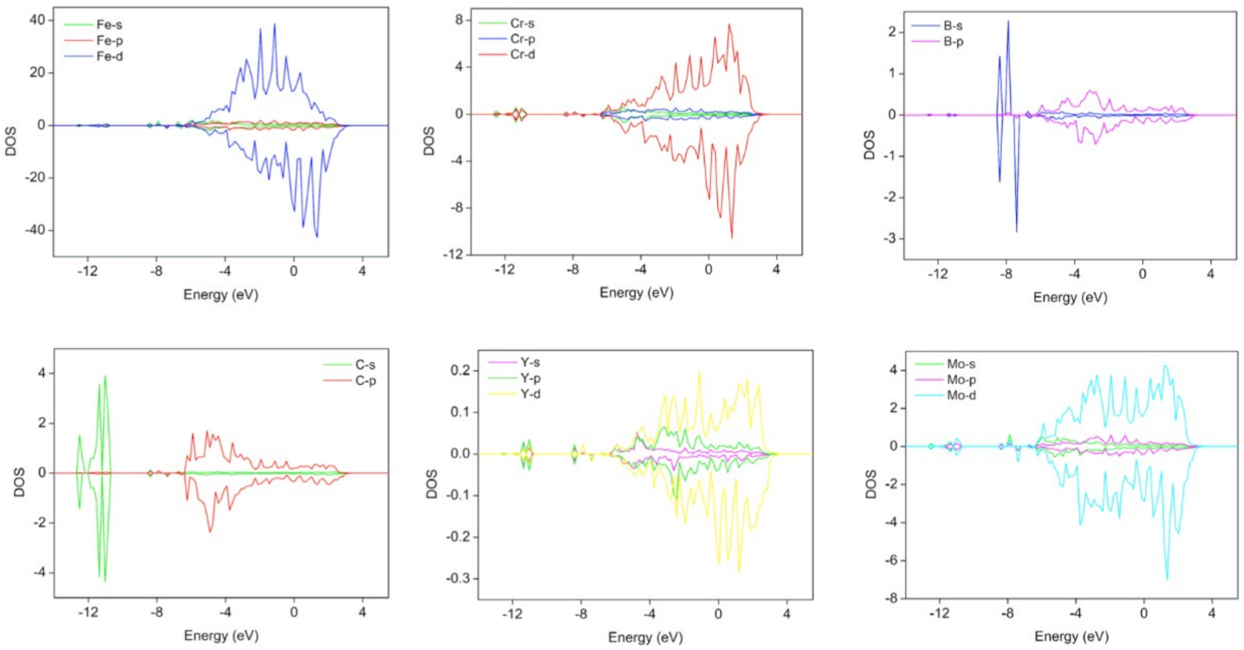

Fig. S8 PDOS structures of each atom in the H-OH-BMG phase.

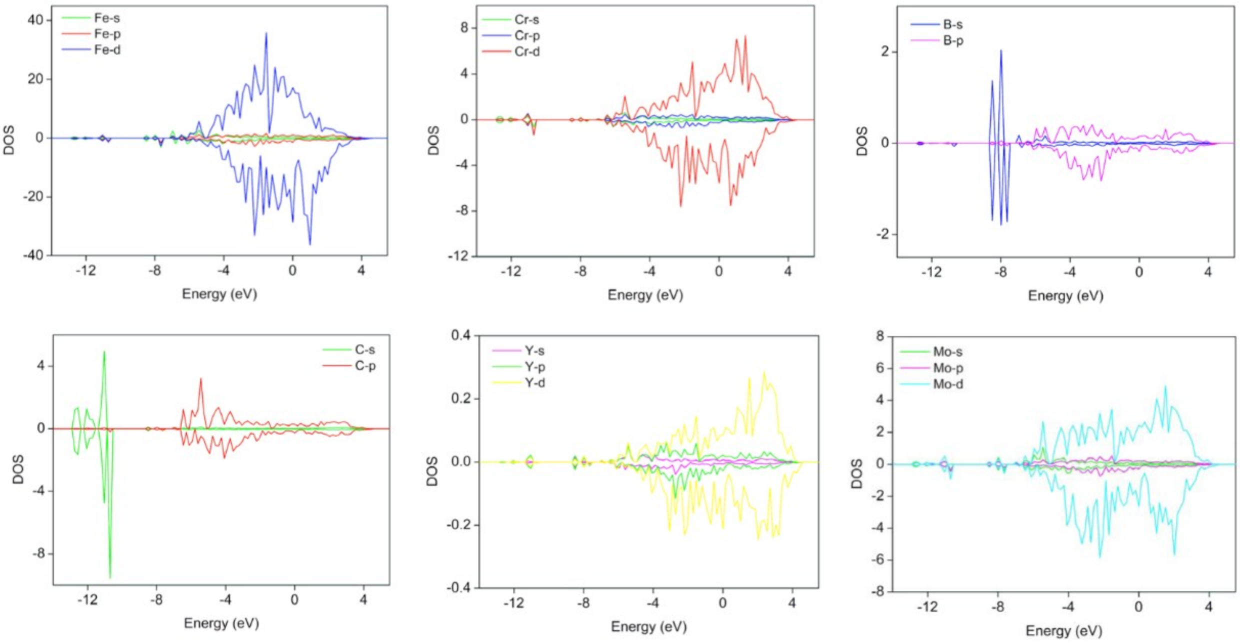

Fig. S9 PDOS structures of each atom in the H_2O-H-OH-BMG phase.

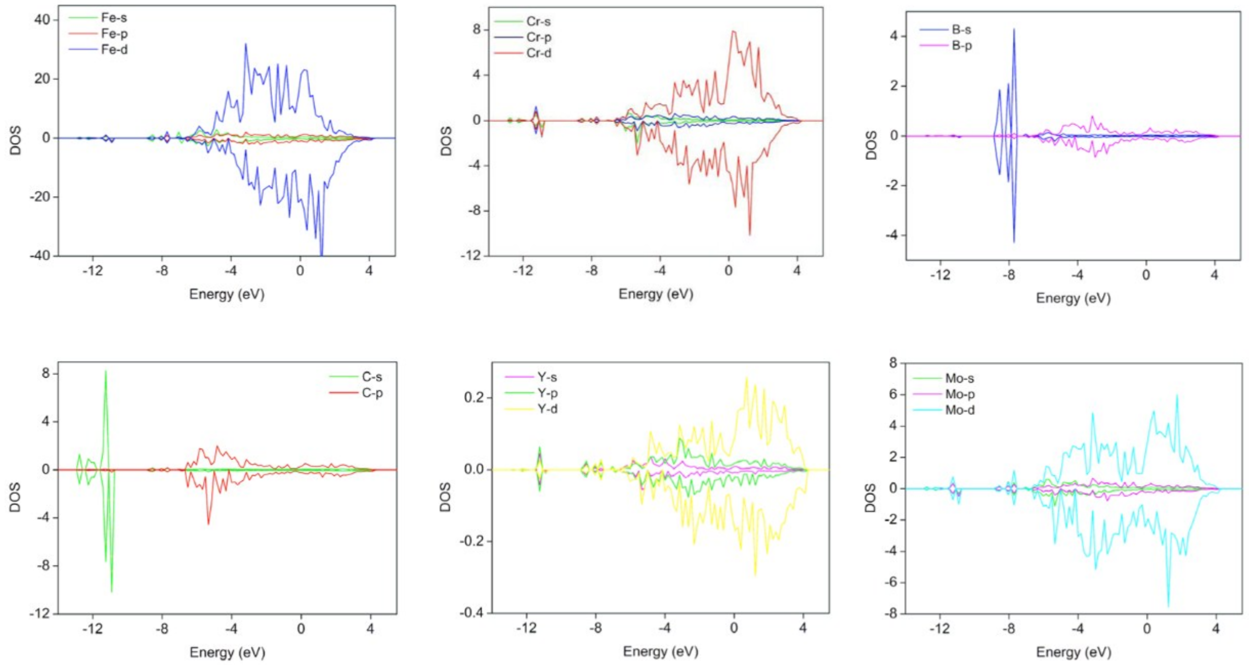

Fig. S10 PDOS structures of each atom in the 2H-2OH-BMG phase.

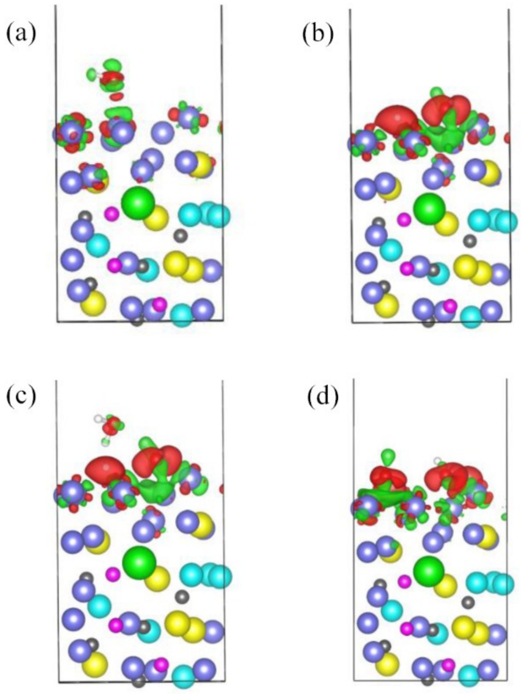

Fig. S11 Differential charge density distributions of (a) H_2O, (b) H+OH, (c) H_2O-H-OH, and (d) 2H+2OH on the BMG surface. Color coding consists of red for charge accumulation and green for charge depletion (isovalue = 0.005 e/Å^3).

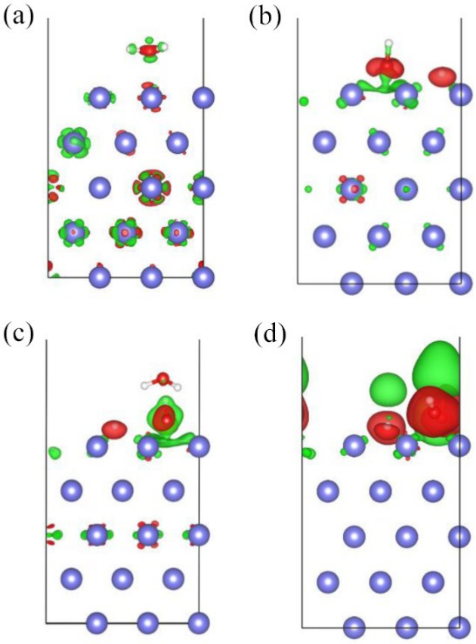

Fig. S12 Differential charge density distributions of (a) H_2O, (b) H+OH, (c) H_2O-H-OH, and (d) 2H+2OH on the Fe(110) surface. Color coding consists of red for charge accumulation and green for charge depletion (isovalue = 0.005 e/Å^3).

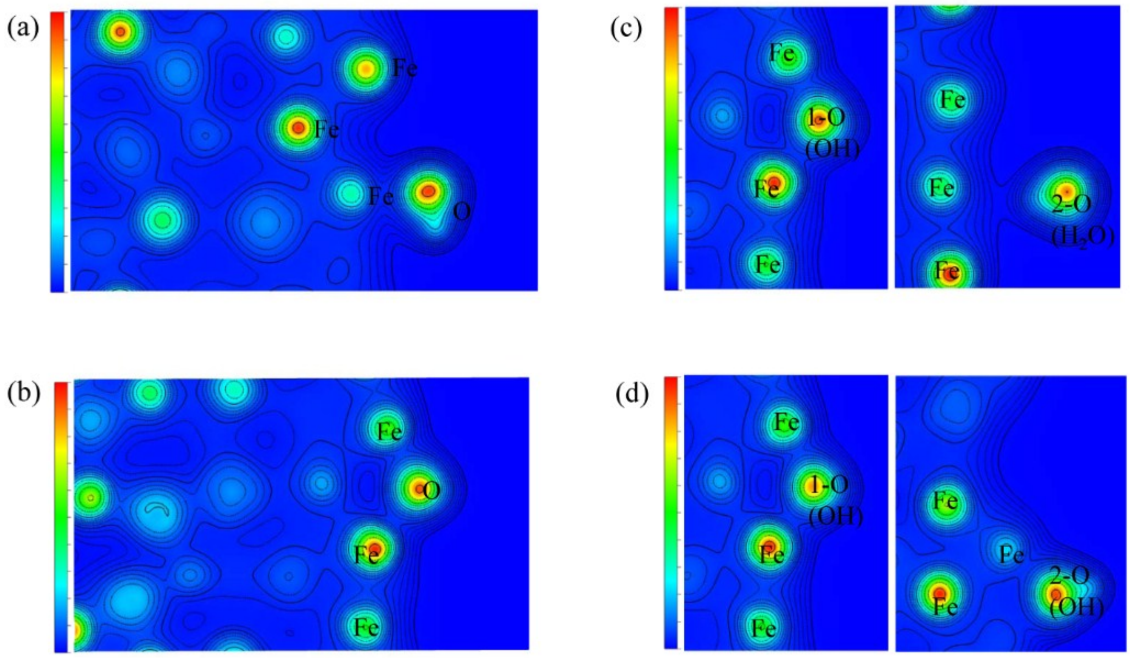

Fig. S13 Electrostatic potential plots of (a) H_2O, (b) H+OH, (c) H_2O-H-OH, and (d) 2H+2OH on the BMG surface viewed from the (010) plane.

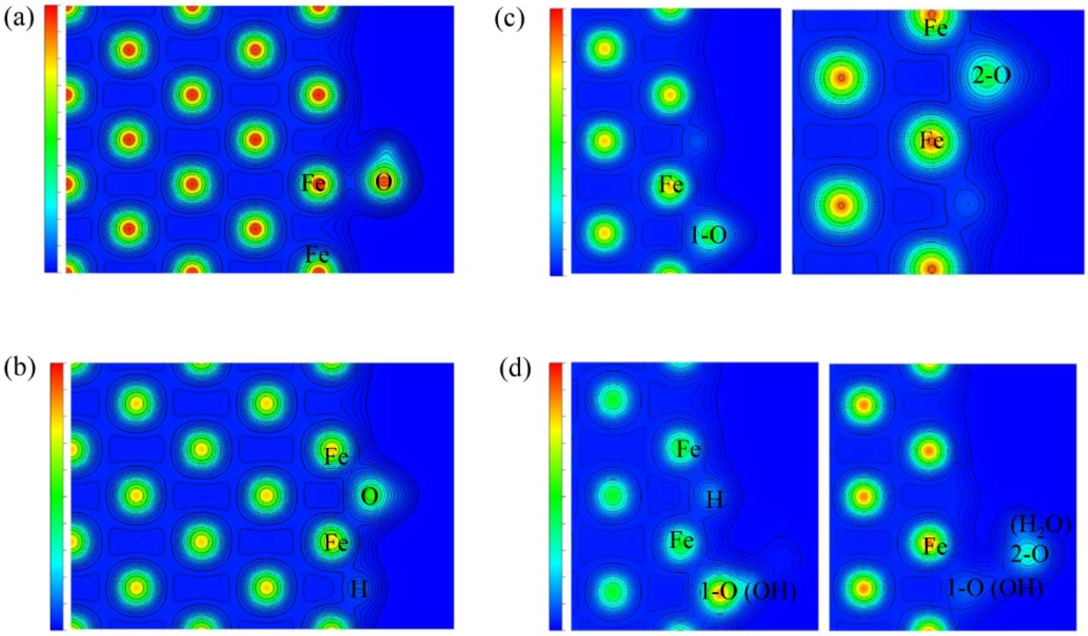

Fig. S14 Electrostatic potential plots of (a) H_2O, (b) H+OH, (c) H_2O-H-OH, and (d) 2H+2OH on the Fe(110) surface viewed from the (110) plane.

Reference

1. H. Arora, H. Grewal, M. Veligatla, H. Singh and S. Mukherjee, *Surf. Eng.*, 2014, **30**, 779-783.
2. C. Zhang, W. Wang, Y.-C. Li, Y.-G. Yang, Y. Wu and L. Liu, *J. Mater. Chem. A*, 2018, **6**, 6800-6805.
3. G. Duan, D. Xu, Q. Zhang, G. Zhang, T. Cagin, W. L. Johnson and W. A. Goddard III, *Phys. Rev. B*, 2005, **71**, 224208.
4. J. Farmer, T. Omlor, S. Menon and L. Brewer, *Long-Term Corrosion Resistance of Iron-Based Amorphous Metal Coatings*, Lawrence Livermore National Lab.(LLNL), Livermore, CA (United States), 2011.
5. S. S. B. R. Ramachandran, C. D. Wick, *4th Annual Conference on Materials Science, Metals, and Manufacturing (M3)*, 2017, Global Science and Technology Forum, Singapore, DOI: 10.5176/2251-1857_M5317.5120.
6. H. Ni, X. Liu, X. Chang, W. Hou, W. Liu and J. Wang, *J. Alloy. Compd.*, 2009, **467**, 163-167.
7. C. Qing-Jun, S. Jun, F. Hong-Bo, S. Jian-Fei, H. Yong-Jiang and D. Mccartney, *Chinese Phys. Lett.*, 2005, **22**, 1736.
8. V. Y. Kazimirov, *Phys. Rev. B*, 2009, **80**, 214117.
9. A. Grottesi, M. A. Ceruso, A. Colosimo and A. Di Nola, *Proteins.*, 2002, **46**, 287-294.